HHS Public Access

Author manuscript

Biochem Pharmacol. Author manuscript; available in PMC 2019 June 01.

Published in final edited form as:

Biochem Pharmacol. 2018 June ; 152: 187–200. doi:10.1016/j.bcp.2018.03.027.

Novel Regulations of the Angiotensin II Receptor Type 1 by Calmodulin

Kevin Ehlers[1], **Robert Clements**[1], **Mark VerMeer**, **Jennifer Giles**, and **Quang-Kim Tran**[*]

Department of Physiology & Pharmacology, Des Moines University Osteopathic Medical Center, 3200 Grand Avenue, Des Moines, IA 50312

Abstract

The angiotensin II receptor type 1 (AT_1R) mediates many Ca^{2+}-dependent actions of angiotensin II (AngII). Calmodulin (CaM) is a key transducer of Ca^{2+} signals in cells. Two locations on the receptor's submembrane domains (SMD) 3 and 4 are known to interact with CaM. However, the binding sites for CaM, biochemical properties of the interactions, and their functional impact are not fully understood. Using a FRET-based screening method, we identified a new binding site for CaM on SMD2 (a.a. 125–141), in addition to SMD3 and the juxtamembranous region of SMD4 ($SMD4_{JM}$, a.a., 309–327). Simultaneous measurements of CaM binding and free Ca^{2+} show that the interactions are Ca^{2+}-dependent, with disparate K_d and EC50(Ca^{2+}) values within the physiological range of cytoplasmic Ca^{2+}. Full interaction between CaM and SMD3 requires the entire domain (a.a. 215–242) and has an EC50(Ca^{2+}) value in the range of resting cytoplasmic Ca^{2+}, suggesting AT_1R-CaM interaction can occur in resting conditions in cells. AngII induces robust ERK1/2 phosphorylation in primary vascular smooth muscle cells. This effect is suppressed by AT_1R inhibitor losartan and virtually abolished by CaM antagonist W-7. AngII-induced ERK1/2 phosphorylation is suppressed in cells expressing mutant AT_1R with reduced CaM binding at each identified binding domain. AngII triggers transient Ca^{2+} signals in cells expressing wild-type AT_1R. These signals are reduced in cells expressing mutant AT_1R with reduced CaM binding at SMD3 or $SMD4_{JM}$, but are very slow-rising, low amplitude signal in cells expressing AT_1R with reduced CaM binding at SMD2. The data indicate that CaM interactions with AT_1R can occur at various domains, with different affinities, at different physiological Ca^{2+} levels, and are important for AT_1R-mediated signaling.

Graphical Abstract

[*]Corresponding author: Quang-Kim Tran, Department of Physiology & Pharmacology, Des Moines University Osteopathic Medical Center, Ryan Hall 258, 3200 Grand Avenue, Des Moines, IA 50312, Tel: 515-271-7849; Fax: 515-2714219, kim.tran@dmu.edu.
[1]Equal contributions.

Conflict of Interest

None declared.

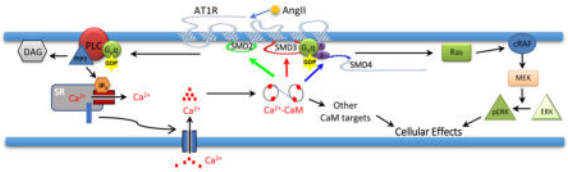

Keywords

Angiotensin II receptor type 1; calmodulin; calcium; FRET biosensor; angiotensin II

1. Introduction

Angiotensin II (AngII) is among the most potent vasoactive substances produced in humans. Its effects are numerous, from vasoconstriction to control of fluid and electrolytes balances. Many of the physiological and pathological effects of AngII are mediated by the angiotensin II receptor type 1A (AT_1R). Activation of AT_1R triggers cardiovascular remodeling in subjects with hypertension and heart failure [19]. Pharmacological inhibition of AT_1R has been exploited extensively in the treatment of hypertension and heart failure. Classically, AT_1R is a 7-pass transmembrane receptor associated with $G\alpha_{q/11}$, whose dissociation upon AngII binding to AT_1R is associated with increases in intracellular free Ca^{2+} concentration, followed by both pre-genomic actions such as contractions of the heart and muscle cells and genomic actions that alter the expression of various genes [17]. AT_1R also interacts with β-arrestin, triggering a G protein-independent cascade of downstream events, with distinct physiological outcomes [11]. Additionally, the activities of AT_1R are regulated by receptor-interacting proteins [1, 6, 32]. Nevertheless, aspects of signaling via AT_1R at the receptor level and its regulatory inputs remain incompletely understood.

Calmodulin is a ubiquitous transducer of intracellular Ca^{2+} signals. It is estimated to bind up to 300 intracellular proteins [21]. Despite its universal requirement, CaM is not expressed sufficiently for all its binding sites within the cell [10]. Shortage of CaM relative to its binding sites [12, 14, 23, 24, 31], coupled with disparate binding affinities for its target proteins from ~ 10^{-11} – 10^{-5} M, has made CaM a target for dynamic competition among its binding proteins, leading to new modes of functional coupling in cells [23, 24]. Over the last two decades, CaM has been shown to interact with several GPCRs, such as the metabotropic glutamate receptors mGluR1 and mGluR5 [18], opioid μ receptors [30], the parathyroid hormone receptor 1 [15], the 5-HT(1A) and 5-HT(2C) receptors [3, 28], the D_2 dopamine receptors [7], AT_1R [22, 32], and the G protein-coupled estrogen receptor 1 (GPER) [25, 27]. CaM binding to the 5-HT(1A) alters receptor phosphorylation and G protein coupling [28]; while its association with 5-HT(2C) and GPER is important receptor-mediated ERK1/2 activation [3, 25]. In 1999, a CaM-binding domain was identified at the juxtamembranous region of the 4th submembrane domain ($SMD4_{JM}$) of AT_1R (a.a. 305–327, rat sequence) [22]. The interaction was shown to be Ca^{2+}-dependent. In 2013, Zhang et al. identified another CaM-binding domain on SMD3 (a.a. 215–232) and confirmed the previously identified domain on the juxtamembranous domain of the 4th submembrane domain of the receptor [32]. In that work, CaM was shown to compete for $G_{\beta\gamma}$ association with both the

partial SMD3 and $SMD4_{JM}$ peptides *in vitro*, indicating a role for CaM binding in $G_{\beta\gamma}$ coupling.

Despite identification of two CaM-binding domains on AT_1R, questions remain to be answered regarding total number of binding sites, biochemical properties and regulatory inputs of the interactions with CaM. Additionally, the functional impact of these interactions in cells are unknown. For example, are segments a.a. 305–327 (rat) in $SMD4_{JM}$ [22] and a.a. 215–232 (rat sequence) in SMD3 [32] the only locations where CaM interacts with AT_1R? How much Ca^{2+} is needed for these interactions to occur? In this regard, for most known CaM-GPCR interactions, information is only available whether CaM binding to GPCR domains occurs in saturating Ca^{2+} or absence of Ca^{2+}. The lack of $EC50(Ca^{2+})$ values for CaM-GPCR domain interactions makes it difficult to predict when an interaction occurs in cells. Additionally, what are the functional implications of AT_1R-CaM interactions? We recently used a FRET-based method to identify and characterize four distinct CaM-binding domains in the G protein-coupled estrogen receptor 1 (GPER) [27]. The method is highly specific and allows for precise determinations of apparent K_d values of CaM binding to the GPCR domains as inserts between the donor-acceptor FRET pair. These values serve as sensitive parameters to determine the binding domains, especially those that do not conform to any known binding motifs. Simultaneous measurements of biosensor-CaM interaction and responses of suitable Ca^{2+} indicator also enables determination of the precise $EC50(Ca^{2+})$ values of the interactions. These values, coupled with measured free Ca^{2+} concentrations in cells, enable predictions of the physiological scenarios in which a particular CaM GPCR interaction may occur [27].

In this study, we have generated new FRET reporters to screen all submembrane domains of AT_1R for interactions with CaM. We identified a new CaM-binding domain on the receptor'sSMD2 (a.a. 125 – 141), confirmed interactions at $SMD4_{JM}$ (a.a. 309 – 327) and characterized the full interacting domain in SMD3. All three domains interact with CaM in a Ca^{2+}-dependent fashion. $EC50(Ca^{2+})$ values determined for each specific interaction by simultaneous measurements of biosensor responses and free Ca^{2+} indicate that AT_1R-CaM binding at different SMDs can take place at drastically different physiological Ca^{2+} concentrations in the cell. Mutagenesis studies were used *in vitro* and in cells to examine the functional impact of CaM binding at the individual sites on AT_1R-mediated signaling.

2. Materials and Methods

2.1. Materials

All molecular biology enzymes and competent cells were from New England Biolabs (Ipswich, MA). RNeasy kit was from Qiagen. High Capacity cDNA reverse transcription kit was from Applied Biosystems (Foster City, CA). Fetal bovine serum, isopropyl β-D-1-thiogalactopyranoside, and M-199 culture medium were obtained from Sigma-Aldrich (St. Louis, MO). HisPur cobalt resin was from Thermo Fisher (Waltham, MA). Phenyl Sepharose CL-4B resin was from GE Healthcare Life Sciences (Milwaukee, MI). DMEM culture medium was from Caisson Laboratories (Smithfield, UT). Polyethylenimine and penicillin/streptomycin were from ThermoFisher (Carlsbad, CA). Fura-2/AM was purchased from Teflabs (Austin, TX). Ionomycin, indo-1, XRhod-5F, collagenase type A, papain and

dithiothreitol were obtained from ThermoFisher Scientific (Carlsbad, CA). Angiotensin II peptide, W-7 and losartan potassium were from Sigma Aldrich (St. Louis, MO). Pierce™ BCA protein assay kit, enhanced chemiluminescence detection kit, and Br2BAPTA were from ThermoScientific (Carlsbad, CA). Bovine serum albumin (BSA) was from Research Products International Corp. (Mt. Prospect, IL). Anti-β actin antibody was from ThermoScientific (RB9421P1). Anti-smooth muscle α actin antibody was from Abcam (ab5694, Cambridge, MA). Anti-ERK1/2 antibody was from Santa Cruz Biotechnology (SC514302, Santa Cruz, CA). Anti-phospho-p44/42 MAPK mouse monoclonal antibody (L34F12) and rabbit anti-hemagglutinin (HA, C29F4) antibody were obtained from Cell Signaling Technology (Danvers, MA).

2.2. Molecular Biology

Total mRNA from HEK 293 cells was isolated using the RNeasy mini kit. Full-length human AT_1R was reverse transcribed from this total mRNA at 100 ng/μL RNA using the High Capacity cDNA reverse transcription kit. To clone AT_1R in frame, a BamHI restriction site was incorporated into the N-terminus of the receptor, while a stop codon followed by an XhoI restriction site was incorporated into its C-terminus. Primers for this reaction are listed in Table-1. The BamHI- AT_1R-XhoI sequence was then cloned into a pcDNA3.1 mammalian expression vector downstream a hemagglutinin (HA) epitope tag as previously described [27].

Constructs for FRET-based biosensors to screen for CaM binding domains in AT_1R were generated as described previously for GPER [27]. Insert sequences from AT_1R's submembrane domains or fragments thereof were PCR amplified from the full-length AT_1R sequence, with incorporation of the KpnI and AgeI restriction sites to the N- and C-terminal ends of the sequences. The insert sequences were then substituted in frame in between the citrine EYFP ($EYFP_c$)-ECFP pair of previously reported pET bacterial expression vectors that encode GPER biosensors [25, 27] to generate biosensor for AT_1R. As with previously described biosensors for GPER, we used the $BSAT_1R_x$ nomenclature, where x denotes the amino acid sequence (human) of the AT_1R fragment used as biosensor insert. Biosensors and primers are listed in Table-1.

Substitutions in the submembrane domains of AT_1R to reduce CaM binding were generated by incorporating gBlock gene fragments containing the desired sequence (IDTDNA, Coraville, IA) in frame into the full-length receptor. The SMD wild-type and mutant amino acid sequences are listed in Table-2. Gblock gene fragments for the mutant sequences as well as restriction enzymes used to clone the mutant domains in frame to full-length AT_1R are listed in Table-3. Mutant biosensors were subsequently generated by PCR amplifying SMD sequences from the full-length mutant AT_1R, followed by incorporation of these sequences in between the $EYFP_c$-ECFP pair as described above. Primers to generate the mutant inserts are listed in Table-1.

To generate fusions between mKate2 and wild-type or mutant AT_1R, mKate2 was PCR amplified from the pDONR-P4-P1-mKate2 plasmid, a gift from Dr Planas, Institut d'Investigacions Biomediques de Barcelona (Addgene.org). The KpnI and BamHI restriction sites were incorporated into the N- and C-terminal ends of mKate2. This fragment

was then substituted for the HA tag in the HA-AT_1R fusions. All constructs were verified by DNA sequencing (University of Missouri).

2.3. Expression and purification of proteins

pET plasmids encoding biosensors and CaM were expressed in BL21(DE3) cells. Biosensors and CaM were purified as described in detail previously [25, 27].

2.4. Screening for CaM-binding domains in AT_1R using $BSAT_1R_X$

Purified $BSAT_1R_X$ were mixed at 22°C with titration buffer (25 mM Tris, 100 mM KCl, pH 7.5), 0.1 mg/mL bovine serum albumin and 1 mM $CaCl_2$ in a quartz cuvette (Hellma Analytics, Plainview, NY). Incremental purified CaM was added to the mixture as $BSAT_1R_X$ fluorescence spectra were monitored in a QuantaMaster™-40 spectrofluorometer (Photon Technology International, Inc., Birmingham, NJ). Direct interaction between Ca^{2+}-CaM and $BSAT_1R_X$ insert was defined by disruption of FRET between ECFP and $EYFP_c$, manifested as an increase in ECFP emission, a decrease in $EYFP_c$ emission and crossing of ECFP and $EYFP_c$ spectra at the isoemissive point (~510 nm). $BSAT_1R_X$ fractional responses were determined by the formula

$$BS_{fract} = \frac{R - R_{\min}}{R_{\max} - R} \quad (1)$$

where R_{min} and R_{max} are the ratios between emission intensities at λ475 and λ535 nm (F475/F535) when the biosensor is in unbound and maximally bound state, respectively. Dilution due to addition of CaM was minimal, yet was calculated using a detailed excel spreadsheet algorithm; however, the use of ratio in formula (1) negated the need to correct for dilution. Fractional biosensor responses were plotted against titrated CaM concentrations. Apparent K_d values of $BSAT_1R_X$-CaM interactions were obtained by fitting fractional responses as a function of CaM concentration to a hyperbolic or quadratic binding equations as described [20, 27]:

$$BS_{fract} = \frac{[CaM]_{tot}}{[CaM]_{tot} - K_d} \quad (2)$$

$$BS_{fract} = \frac{[BS] - [CaM] - K_d - \sqrt{([BS] + [CaM] + K_d)^2 - 4[BS][CaM]}}{2[BS]} \quad (3)$$

where BS_{fract}, [BS] and [CaM] are $BSAT_1R_X$ fractional response, total concentration of $BSAT_1R_X$ and CaM in the reaction mix, respectively.

2.5. Measurement of Ca^{2+} sensitivities of AT_1R-CaM interactions

Ca^{2+} sensitivities of the interactions between CaM and different submembrane domains of $BSAT_1R_X$ were measured by simultaneously monitoring the responses of a suitable Ca^{2+} indicator and $BSAT_1R_X$ in the presence of saturating CaM concentration (determined from K_d titrations) and incremental increases in added Ca^{2+}. Starting reaction mixture contained 0.5 μM $BSAT_1R_X$, 2 μM Ca^{2+} indicator, 0.1 mg/ml BSA, 0.25 mM Br2BAPTA, and saturating CaM concentration (determined from K_d determinations), in titration buffer at 22°C. The choice of suitable Ca^{2+} indicators were made by initially comparing the responses of $BSAT_1R_X$ and a Ca^{2+} indicator to achieve relatively consistent response ranges as Ca^{2+} was titrated in the mixture. For example, a Ca^{2+} indicator whose response was saturated before $BSAT_1R_X$ begins to respond, or vice-versa, would be unsuitable for measurement of Ca^{2+} sensitivity. These initial titrations identified XRhod-5F (K_d for Ca^{2+} = 1.6 μM) and indo-1 (K_d for Ca^{2+} = 0.23 μM) as suitable indicators for $BSAT_1R_X$. For XRhod-5F, free Ca^{2+} concentrations were determined by its emission intensity at λ600nm with excitation at λ580 nm, measured simultaneously with $BSAT_1R_X$ responses. Dilution factors, though minimal, were carefully recorded on an Excel spreadsheet for each addition of Ca^{2+} and used to correct for emission intensity. Free Ca^{2+} values were calculated using the formula

$$[Ca^{2+}](\mu M) = 1.6 \times \frac{F - F_{\min}}{F_{\max} - F} \quad (4)$$

where, 1.6 is the in vitro K_d value of XRhod-5F for Ca^{2+}; F_{min} and F_{max} are XRhod-5F emission intensities at λ600nm under nominally Ca^{2+}-free and Ca^{2+}-saturating conditions, respectively. For indo-1, indicator responses were obtained as ratios between emission intensities at λ405nm and λ485nm, with excitation at λ340nm. Free Ca^{2+} values were calculated from these ratios using the formula

$$[Ca^{2+}](\mu M) = 0.23 \times \frac{R - R_{\min}}{R_{\max} - R} \quad (5)$$

where 0.23 is the in vitro K_d of indo-1 for Ca^{2+} in μM, R is the ratio between indo-1 emission intensities at λ405nm and λ485nm, R_{min} and R_{max} are the F405/F485 ratios obtained at nominally Ca^{2+}-free and Ca^{2+}-saturating conditions, respectively.

Ca^{2+} sensitivities of $BSAT_1R_X$-CaM interactions were determined by the EC50(Ca^{2+}) values, derived from fits of $BSAT_1R_X$ fractional responses (eq. 1) as a function of free Ca^{2+} using the equation:

$$BS_{fract} = \frac{[Ca^{2+}]^n_{free}}{[Ca^{2+}]^n_{free} + [EC_{50}(Ca^{2+})]^n} \quad (6)$$

where BS_{fract} is obtained from equation (1); n is the Hill coefficient.

2.6. Cell isolation and culture

Primary VSMCs were isolated from descending section of porcine thoracic aortas based on a modification of the methods published by Bolzon, Ulrich-Merzenich and Leik as recently described [8, 13, 27, 29]. Descending porcine thoracic aortas were obtained fresh from a local slaughter house and transported in sterile phosphate buffered saline containing 3% penicillin/streptomycin. After removal of perivascular adipose tissue, the aortas were cut open and endothelial cells were removed by mechanical scraping and short incubation with 0.02% collagenase, 0.1% papain and 4 mM dithiothreitol and re-scraping. After rinsing in sterile PBS, the aortas were dissected into strips and the luminal surface was incubated with the enzyme mix for 90 minutes at 37°C. The luminal surface was subsequently scraped again, and cells from this treatment were grown in M-199 medium containing 10% fetal bovine medium and 2% penicillin/streptomycin in 90% humidified condition with 5% CO_2 at 37°C for one week. This approach consistently yields highly homologous populations of VSMCs, verified by both morphological features and smooth muscle α-actin expression. VSMCs were used for 2–3 passages after isolation. The protocol was approved by Des Moines University Institutional Biosafety Committee. Immortalized human embryonic kidney (HEK293) cells were purchased from ATCC (CRL-1573, initial passage 15) and cultured in DMEM medium containing and 10% fetal bovine serum. Cells were used for up to 15 passages from the initial stock from vendor.

2.7. Transfection

HEK293 cells were transfected with plasmids encoding mKate2 in isolation or fused with wild-type or mutant full-length AT_1R using polyethylenimine (PEI) based on a modification of the method published by Aricescu et al. [2]. Briefly, HEK293 cells were grown to 60% confluency by the time of transfection. Plasmid DNA and PEI were allowed to form a complex at room temperature at a PEI:DNA mass ratio of 1.5:1 for 20 minutes in serum-free, antibiotic-free culture medium (DMEM or M-199). The cells were subsequently incubated with 1:5 vol/vol DNA-PEI complex in DMEM containing 2% FBS for 6 hours before medium was replaced by regular culture medium. The cells were cultured for another 12 hrs before experimentation.

2.8. Western Blotting

All cell treatments were performed at room temperature in modified Tyrode's buffer(composition in mM: 150 NaCl, 2.7 KCl, 1.2 KH_2PO_4, 1.2 $MgSO_4$, 10 HEPES, pH 7.5) containing 1.5 mM $CaCl_2$. Following treatment and cell lysis, the protein content was measured using BCA assay performed in triplicate for all samples. All lanes in each gel were loaded with equal amounts of total proteins, adjusted for detectability with each antibody. After detection of the levels of ERK1/2 phosphorylation, the same membrane fragments were stripped and reprobed for total ERK1/2. Following secondary incubation, membrane fragments were developed using enhanced chemiluminescence in a ChemiDoc™ XRS+ imaging system (Bio-Rad). Image Lab 5.0 software (Bio-Rad) was used for densitometry. Densitometric values of phosphorylated ERK1/2 bands were corrected for corresponding values of total ERK1/2 bands and normalized to control values.

2.9. Measurement of intracellular Ca^{2+} concentration in HEK293 cells expressing mKate2-AT_1R

Intracellular Ca^{2+} concentration was measured in HEK293 cells expressing mKate2 only or mKate2 in fusion with wild-type or mutant full-length AT_1R as described previously [25, 26]. HEK293 cells were loaded with 4 μM fura-2/AM for 30 min in culture medium at 37°C. After removal of fura-2/AM, the cells were equilibrated in modified Tyrode's buffer (composition in mM: 150 NaCl, 2.7 KCl, 1.2 $KH2PO_4$, 1.2 $MgSO_4$, 10 HEPES, 1 $CaCl_2$, pH 7.4) for 15 min at room temperature. mKate2 fluorescence was first identified and selected in RFP channel. Filter cube was then switched to fura-2 channel without changing the microscopic field. Excitation of fura-2 was alternated between λ340 nm and λ380 nm for 100 ms per 1-s cycle from an ultra-high speed wavelength switcher (Lambda DG-4, Sutters Instruments) at 1-ms switching interval. Emission at λ510 nm was collected via an EMCCD camera (DU-885, Andor Technology). At the end of the agonist-induced Ca^{2+} signal time course, R_{max} values of fura-2 were obtained in all cells by adding 10 μM ionomycin and 10 mM $CaCl_2$. R_{min} values were determined in all cells using a previously developed equation [26]. Free Ca^{2+} concentrations were calculated using the standard equation

$$Ca^{2+}(nM) = K_d \times \frac{S_f}{S_b} \times \frac{R - R_{\min}}{R_{\max} - R} \quad (7)$$

Where the K_d value is 224 nM for fura-2; R is the observed fura-2 ratio during the experiments. S_f and S_b represent the emission intensities at λ510 nm corresponding to the Ca^{2+}-free and Ca^{2+}-bound states of fura-2. S_b values were readily measured in all cells together with R_{max} values. S_f values were determined in each cell using a previously developed equation [26].

2.10. Statistical Analysis

Data were normally distributed and are expressed as means ± SD. Statistical analysis was performed using one-way ANOVA, followed by a Tukey *post-hoc* test. Statistical significance was set at $P < 0.05$.

3. Results

3.1. Screening for all CaM-binding domains in AT_1R

The two known CaM-binding domains in AT_1R include a.a. 215–232 in SMD3 and a.a. 305–327 in $SMD4_{JM}$ [22, 32]. To confirm and screen for all CaM-binding sites on AT_1R, we used a FRET-based approach to screen for CaM-binding sites in the submembrane domains of human AT_1R. This method has allowed us to identify four distinct CaM-binding sites on the four submembrane domains of GPER, some of which do not conform to any known CaM-binding motifs [27]. We generated a host of FRET biosensors that consist of partial or full-length submembrane domains of AT_1R flanked by the FRET donor ECFP and acceptor citrine EYFP ($EYFP_c$). These included $BSAT_1R_{52–64}$ (covering SMD1), $BSAT_1R_{125–141}$,

(covering SMD2), $BSAT_1R_{215–232}$ (covering previously identified CaM-binding domain in SMD3 [32]), $BSAT_1R_{215–242}$ (covering the entire SMD3), and a series of $BSAT_1R_X$ to scan SMD4 due to the length of this domain (Table-1). Figures 1A–B recapitulate the principle of the biosensors for screening of CaM-binding sequences. A domain to be screened for CaM binding is inserted between $EYFP_c$-ECFP (see also Materials and Methods). In the absence of CaM interaction with the insert sequence, proximity between $EYFP_c$ and ECFP allows for robust FRET between them upon excitation of the ECFP moiety (430 nm) (Fig. 1A). Specific interaction between CaM and the insert domain will disrupt FRET (Fig. 1B), causing an increase in ECFP emission, a decrease in EYFP emission, and crossing of the emission spectra at the isoemissive point (~510 nm) [27]. In the absence of specific binding with the insert, up to 700 μM CaM caused no emission spectral changes of the FRET pair [27]. With high sensitivity of FRET change in response to conformational changes of the insert upon CaM binding, it is easy to determine with high precision the apparent binding affinities between CaM and the insert domain in biosensor format. The length of the insert domain can be varied until the highest binding affinity is achieved, which identifies the correct domain required for full interaction with CaM. Figure 1C shows a Coomassie gel of the biosensors characterized. Figure 1D shows Coomassie staining of three separate preparations of CaM used to screen CaM binding. All proteins showed as single bands on the gels, demonstrating high purity.

Using these biosensors, our first goal was to confirm the reported interactions at a.a. 305–327 on $SMD4_{JM}$ and a.a. 215–232 on SMD3 and to screen for any other sites of interactions on the submembrane domains. As reported interactions were Ca^{2+}-dependent, all screens were first done with Ca^{2+}-liganded purified CaM. $BSAT_1R_{52–64}$ (covering SMD1) did not interact with CaM; its emission spectra virtually overlapped in response to buffer alone or high concentration of CaM (Fig. 2A). Surprisingly, $BSAT_1R_{125–141}$, which covers SMD2, demonstrated clear signature spectral changes upon Ca^{2+}-CaM titration (Fig. 2B). Initial screenings for the entire SMD4 sequence using $BSAT_1R_X$ spanning a.a. 304–323, 305–327, 309–327, and 328–359 indicated that $BSAT_1R_{328–359}$ does not interact with CaM (not shown), while $BSAT_1R_{309–327}$ possesses the highest affinity for interaction with CaM of all $BSAT_1R_X$ covering the $SMD4_{JM}$ region. Figure 2C shows the signature spectral changes for positive interaction upon titration of Ca^{2+}-liganded CaM into $BSAT_1R_{309–327}$. $BSAT_1R_{215–232}$ also showed positive responses to Ca^{2+}-liganded CaM, confirming previously reported results on this segment [32] (Fig. 2D). Since a.a. 215–232 only represents a portion of SMD3, we questioned if this represents the entire CaM-binding domain here. $BSAT_1R_{215–242}$, which covers the entire SMD3, clearly binds CaM (Fig. 2E). However, $BSAT_1R_{215–242}$ has a 3-fold higher affinity for Ca^{2+}-CaM than $BSAT_1R_{215–232}$, indicating that full interaction with CaM requires the entire SMD3 (Fig. 2F). Figure 2G shows fractional saturation of $BSAT_1R_{125–141}$, $BSAT_1R_{215–242}$, and $BSAT_1R_{309–327}$ as a function of Ca^{2+}-liganded CaM. The apparent K_d values for these interactions are shown in Table-4.

We previously described the parameter dynamic range (DR), determined as the maximal change in FRET ratio of the biosensors [27]. CaM causes significant conformational changes in its target proteins upon binding, a property important for its role in promoting target activities. The dynamic range of a $BSAT_1R_X$ reflects the conformational changes of

the insert domain that could occur upon interaction with CaM and provides a prediction of the potential conformational change that could take place in the holoreceptor upon CaM binding. Figure 3A shows relative FRET ratios of the $BSAT_1R_X$ as a function of Ca^{2+}-CaM; Fig. 3B shows the increases in dynamic range of the $BSAT_1R_X$ from unbound state (ΔDR). Full interaction with Ca^{2+}-CaM at a.a. 215–242 (SMD3) is apparently associated with the largest dynamic range, followed by that of a.a. 309–327 ($SMD4_{JM}$) and a.a. 125–141 (SMD2). This is similar to the order of affinity of these domains for Ca^{2+}-CaM (Fig. 2G, Table-4).

3.2. Ca^{2+} dependencies and sensitivities of the interactions between AT_1R and CaM

We first examined the Ca^{2+} dependency of the interactions between CaM and the domains identified. Previous studies have demonstrated Ca^{2+} dependency for the interaction at a.a. 305–317 in $SMD4_{JM}$ and a.a. 215–232 in SMD3 by examining binding in the presence of saturating Ca^{2+} or nominal absence of Ca^{2+} using the Ca^{2+} chelator EGTA [22, 32]. Although our initial biosensor screen showed that $BSAT_1R_{125–141}$, $BSAT_1R_{215–242}$, and $BSAT_1R_{309–327}$ all interacted with Ca^{2+}-liganded CaM, it was necessary to examine whether any interactions take place in the absence of Ca^{2+}, since both Ca^{2+}-dependent and independent interactions between CaM and the same binding domain have been shown [4, 5]. Figure 4 shows the spectral changes of $BSAT_1R_{125–141}$, $BSAT_1R_{215–242}$, and $BSAT_1R_{309–327}$ in response to Ca^{2+}-saturated CaM (A, C, E) or apoCaM (B, D, F), at the concentrations that demonstrated maximal binding from the K_d titrations (Fig. 2). At CaM concentrations that produced maximal biosensor response in the presence of Ca^{2+}, no response was observed in the absence of Ca^{2+} (Fig. 4).

Ca^{2+} dependency determined in the presence or absence of saturating concentrations of Ca^{2+} does not allow for predicting when AT_1R-CaM interactions can occur in different physiological scenarios at different free Ca^{2+} levels. Currently, no information exists with respect to the Ca^{2+} sensitivities of these interactions. To measure these parameters, we mixed $BSAT_1R_X$ and CaM in the absence of Ca^{2+} and simultaneously measured responses from both the biosensor and a suitable Ca^{2+} indicator as Ca^{2+} was titrated in the reaction mixture. This approach enables precise determinations of both fractional binding and the free Ca^{2+} concentration at which the binding occurs. The choice of a suitable Ca^{2+} indicator for these titrations was made easy by the commercial availability of many indicators with different K_d values and fluorescent properties. Ideally, a suitable Ca^{2+} indicator will have the same response range with that of $BSAT_1R_X$ to Ca^{2+}-liganded CaM. This can easily be estimated by testing a few Ca^{2+} indicators with different K_d values. Figure 5A shows an example of these measurements. Ca^{2+} was titrated in a mixture of $BSAT_1R_X$, respective saturating CaM (determined from Fig. 2), 0.25 mM BAPTA (to ensure starting condition had essentially no Ca^{2+}), and a Ca^{2+} indicator, in this case indo-1 (K_d for Ca^{2+} =0.23 μM). $BSAT_1R_X$ and Indo-1 responses were simultaneously monitored (Fig. 5A). Free Ca^{2+} was then calculated based on indo-1 response (Eq. (5)) and biosensor fractional saturation was calculated using Eq. (1) and plotted as a function of the corresponding free Ca^{2+} values. A fit from this relationship to Eq. (6) would yield the $EC50(Ca^{2+})$ for the interaction. Indo-1 was used for $BSAT_1R_{215–232}$ and $BSAT_1R_{215–242}$ since initial testing showed the interactions between CaM and these biosensors have the same range of Ca^{2+} sensitivity with

indo-1. XRhod-5F (K_d for Ca^{2+} = 1.6 μM) was used for $BSAT_1R_{125–141}$ and $BSAT_1R_{309–327}$ since its response range was the same with those of the biosensors over the entire Ca^{2+} titration. In these measurements, bleed-through artifacts were avoided by 1) alternate excitation of $BSAT_1R_X$ and Ca^{2+} indicator and 2) well separated excitation wavelengths of indo-1 (340 nm) or XRhod-5F (590 nm) from that of $BSAT_1R_X$ (435 nm). To confirm absence of bleed-through artifacts using this approach for indo-1 and $BSAT_1R_X$, reactions were started with a mixture of indo-1 and $BSAT_1R_{215–242}$ and 0.25 mM BAPTA in the absence of CaM. As incremental Ca^{2+} was added, indo-1 ratio increased until saturation of the signal (Fig. 5B, upper panel) without any alteration in $BSAT_1R_{215–242}$ ratio, which only increased upon addition of purified CaM (Fig. 5B, lower panel). Similarly, absence of bleed-through artifacts was confirmed for XRhod-5F and $BSAT_1R_X$ using the example of $BSAT_1R_{125–141}$ (Fig. 5C). Aggregate plot of $BSAT_1R_X$ fractional saturations as a function of free Ca^{2+} is shown in Fig. 5D. EC50(Ca^{2+}) values for the interactions are listed in Table-4. The order of Ca^{2+} sensitivity these domains for interaction with CaM is a.a. 215–242 (SMD3) > a.a. 309–327 ($SMD4_{JM}$) > a.a. 125–141 (SMD2), similar to the order of binding affinity and dynamic range. Interestingly, EC50(Ca^{2+}) for CaM-$BSAT_1R_{215–242}$ interaction is 150 nM, within the resting Ca^{2+} range in VSMCs. The Ca^{2+} titration curve for CaM-$BSAT_1R_{309–327}$ interaction exhibits a biphasic behavior. Complexes between Ca^{2+}-CaM and a.a. 309–327 ($SMD4_{JM}$) thus apparently consist of two species, CaM-$SMD4_{JM}$Sp1, with an EC50(Ca^{2+}) value of 0.31 ± 0.02 μM, and CaM-$SMD4_{JM}$Sp2, with and EC50(Ca^{2+}) of 3.17 ± 0.2 μM (Table-4).

3.3. CaM-AT_1R interactions are required for AT_1R-mediated ERK1/2 phosphorylation

The data presented so far show that AT_1R possesses three distinct CaM-binding domains with disparate affinities and Ca^{2+} sensitivities for their interactions with CaM. To initially assess the influence of CaM binding on AT_1R-mediated signaling, we tested the effect of inhibiting CaM on AngII-induced ERK1/2 phosphorylation in primary VSMCs. We have routinely isolated primary vascular endothelial cells (PAECs) and then primary VSMCs from the same porcine aortas [25–27]. Under bright-field microscopy, isolated primary PAECs demonstrated typical cobble-stone morphology (Fig. 5A) while the VSMCs demonstrated elongated morphology (Fig. 5B). To confirm the smooth muscle nature of the VSMCs isolated, lysates from PAECs and VSMCs were immunoblotted for smooth muscle α-actin and β-actin. While β-actin was expressed in both lysates, smooth muscle α-actin was only detected in lysate from VSMCs (Fig. 5C). Sub-confluent primary VSMCs were then pretreated for 30 min with vehicle, AT_1R antagonist losartan (1 μM; IC_{50} ~ 5.5 nM), or the CaM antagonist W-7 (100 μM; K_i ~ 20 μM), followed by stimulation with 100 nM AngII for 5 min. AngII triggered robust increases in ERK1/2 phosphorylation. This effect was suppressed by losartan and abolished by W-7 pretreatment (Fig. 6).

The observed effect of W-7, while consistent with a role for CaM binding on AT_1R-mediated signaling, can be non-specific. To assess the role of AT_1R-CaM interaction at individual SMDs, we generated several substitutions in each domain, aiming to reduce CaM binding affinities and Ca^{2+} sensitivities, verified changes in CaM binding affinity and Ca^{2+} sensitivity using biosensor approach, then tested AngII-induced ERK1/2 phosphorylation in cells expressing full-length AT_1R containing wild-type or mutant sequences. The

substitutions introduced in the identified CaM-binding domains are shown in Table-2. $BSAT_1R_{125–141mut}$, $BSAT_1R_{215–242mut}$, $BSAT_1R_{309–327mut}$ all still interact with CaM in a Ca^{2+}-dependent fashion. Figures 7A–C show plots of Ca^{2+}-CaM binding to wild-type vs mutant $BSAT_1R_{125–141mut}$, $BSAT_1R_{215–242mut}$, $BSAT_1R_{309–327mut}$, respectively, demonstrating reductions in CaM binding affinities of all the mutant biosensors. Due to difficulty to saturate binding for $BSAT_1R_{125–141mut}$, Fig. 7A is presented as relative FRET ratio rather than fractional saturation as in Fig. 7B and 7C. Nevertheless, the available titration data clearly shows that $BSAT_1R_{125–141mut}$ has substantially reduced affinity for CaM compared to $BSAT_1R_{125–141}$. Figures 7D–F show fractional responses of the wild-type vs mutant biosensors as a function of free Ca^{2+} determined as described in Fig. 5A. All mutant biosensors showed reduced Ca^{2+} sensitivities for interactions with CaM. The mutant $SMD4_{JM}$ again exhibited a biphasic Ca^{2+} response curve, similar to the wild-type version (Fig. 7F). The apparent K_d and $EC50(Ca^{2+})$ values for CaM interaction with the mutant biosensors are listed in Table-4. Having confirmed the effects of the substitutions to decrease interactions with CaM at each domain, full-length AT_1Rs with wild-type or mutant sequences at each SMD were tagged with a hemagglutinin (HA) epitope tag at their N termini and expressed in HEK293 cells. After 24 hrs, cells were serum starved for 4 hours prior to treatment and lysis. Immunoblotting of samples with the anti-HA antibody showed equal expression levels of the expressed receptors and no bands recognized in the mock-transfected samples (lower immunoblots, Fig. 7G(i), (ii), (iii)). Treatment of mock-transfected HEK293 cells with 100 nM AngII mildly increased ERK1/2 phosphorylation due to the activity of endogenous AT_1R. Heterologous expression of wild-type AT_1R substantially increased this effect. However, in cells expressing AT_1R with the substitutions that were verified to reduce CaM-binding affinity and Ca^{2+} sensitivities (Fig. 7A–F) in SMD2, SMD3, or $SMD4_{JM}$ (upper blots, Fig. 7G, (i), (ii), or (iii), respectively) the effect of AngII was significantly reduced (Fig. 7G, iv). Total ERK1/2 expression levels probed from the same membranes as for ERK1/2 phosphorylation were similar, indicating equal loading (middle blots, Fig. 7G(i), (ii), (iii)).

3.4. CaM-AT_1R interactions are important for AngII-induced Ca^{2+} signals

To corroborate the results with AT_1R-mediated ERK1/2 phosphorylation, we examined the effects of the CaM binding-reducing mutations in the individual SMDs on AngII-induced Ca^{2+} signals. To guarantee Ca^{2+} was measured in cells expressing wild-type or mutant AT_1R, full-length AT_1Rs with wild-type or mutant sequences were fused at their N termini with the fluorescence protein mKate2. N-terminal fusion was chosen to avoid potential interference of mKate2 with important binding partners at the submembrane domain level. HEK293 cells expressing plasmids encoding mKate2 alone or fused with wild-type or mutant AT_1R were loaded with fura-2/AM for Ca^{2+} imaging. mKate2 fluorescence was first identified and marked in the RFP channel (Fig. 8A), followed by switching filter cube for imaging of fura-2 fluorescence in the same microscopic field (Fig. 8B). This guaranteed that Ca^{2+} signals were examined in cells expressing the intended AT_1R version. Merged images (Fig. 8C) show high transfection efficiency. To allow correlation with $EC50(Ca^{2+})$ values determined using purified CaM and $BSAT_1R_X$, measured fura-2 signals were converted to free intracellular Ca^{2+} concentrations (Materials and Methods). To ensure signals were compared among cells expressing equal amounts of wild-type and mutant AT_1R, cells were

selected with mKate2 fluorescence intensities in the same range prior to switching to measurement of Ca^{2+} signals (see also Methods). Figure 8D shows average mKate2 intensity in HEK293 cells expressing mKate2 or mKate2-AT_1R with wild-type or mutant sequences selected for measurement of AngII-induced Ca^{2+} signals. In cells expressing only the mKate2 moiety, 100 nM AngII induced a small Ca^{2+} signal, due most likely to the presence of functional wild-type AT_1R in these cells (our AT_1R cDNA was reverse-transcribed from mRNA isolated from the host HEK293 cells). AngII treatment of cells expressing mKate2 fused with wild-type AT_1R produced a large transient Ca^{2+} signal. The AngII-induced Ca^{2+} signal was reduced in cells expressing mKate2-AT_1R plasmids containing CaM binding-reducing mutations in SMD3 or SMD4. Surprisingly, this signal became a very slow-rising signal with low amplitude, in cells expressing mKate2-AT_1R with mutant sequence on SMD2 (Fig. 8D). To quantitate these signals, integrated areas under curve were calculated for the entire time courses (Fig. 8E). AngII-induced Ca^{2+} signals were significantly reduced in cells expressing mKate2 in fusion with AT_1R containing CaM binding-reducing substitutions in SMD2, 3 or 4 (Fig. 8E). Notably, in the case of AT_1R with mutant SMD2 sequence, the AngII-induced Ca^{2+} signal was very slow-rising and low amplitude, even compared to cells expressing only the mKate2 moiety (Fig. 8D–E).

4. Discussion

In this study, we have identified several new aspects of the interactions between CaM and AT_1R: 1) a new CaM binding site is found spanning a.a. 125–141 on SMD2; 2) full interaction between CaM and SMD3 requires the entire domain, a.a. 215–242; 3) CaM interactions with all three domains require Ca^{2+} and can occur at different Ca^{2+} concentrations in the physiological range, with interaction at a.a. 309–327 in $SMD4_{JM}$ having a biphasic sensitivity to Ca^{2+}; and 4) CaM interaction with each binding site is important for AT_1R-mediated Ca^{2+} signaling and ERK1/2 phosphorylation.

The identification of a.a. 125–141 on SMD2 as a new binding site for CaM on AT_1R is interesting in that the amino acid sequence of SMD2 does not conform to known CaM-binding motifs. This is similar to our identification of SMD1 on GPER as a CaM-binding domain of only 12 residues that can interact with CaM at basal Ca^{2+} levels [27]. The case of AT_1R requiring the entire SMD3 (a.a. 215–242) for full interaction with CaM at this domain is also reminiscent of our observation that fragment a.a. 150–170 of GPER's SMD2 binds CaM, but with a substantially lower affinity than the full-length SMD2, a.a. 150–175, indicating an important role of the basic patch a.a. 170–175 in this process [27]. In the case of AT_1R's SMD3, a.a. 233–242 contains a high percentage of hydrophobic and charged residues, which apparently contribute significantly to CaM binding, adding a 3-fold increase in binding affinity and doubling Ca^{2+} sensitivity for the interaction with the full SMD3, a.a. 215–242, vs the previously reported segment, a.a. 215–232. These findings further support the value of using FRET biosensors to screen for CaM-binding sites in GPCRs.

Simultaneous measurements of $BSAT_1R_X$-CaM interaction and corresponding free Ca^{2+} concentrations indicate that the interactions between CaM and the three identified domains on AT_1R can all occur during a typical cytoplasmic Ca^{2+} signal in VSMCs. With disparate affinities and Ca^{2+} sensitivities, CaM binding may occur at different submembrane domains

at different levels of free Ca^{2+}. SMD3-CaM interaction has an EC50(Ca^{2+}) value of 150 nM (Fig. 5 and Table-4) and at 50 nM free Ca^{2+}, there is significant binding at this domain *in vitro*. These values are well within the resting range of cytoplasmic Ca^{2+} in VSMCs, suggesting that AT_1R-CaM interaction can occur in basal conditions in cells. Considering a competitive environment for CaM among CaM-dependent proteins due to limiting CaM [14, 23–25], CaM interactions with EC50(Ca^{2+}) values in the range of basal Ca^{2+} levels are more likely to occur since fewer target proteins bind CaM at this level of Ca^{2+} compared to during a large Ca^{2+} signals. For the remaining domains, EC50(Ca^{2+}) values of 0.31, 3.18 and 4.1 μM indicate that CaM-$SMD4_{JM}$Sp1, CaM-$SMD4_{JM}$Sp2 and CaM-SMD2 complexes, respectively, are likely to take place at different points during the time course of a typical agonist-stimulated response. Based on Ca^{2+} titration curve, full association between CaM and a.a. 125–141 on SMD2 requires ~ 10 μM free Ca^{2+}. This is attainable in cells, as sub-PM Ca^{2+} in VSMCs reaches 45 μM and remains above 5 μM throughout the time course of the vasopressin-induced Ca^{2+} signal [16].

What are the *in-situ* effects of multi-site CaM associations with AT_1R? Kai et al. showed that synthetic peptides corresponding to residues 125–137 (rat sequence) in SMD2, 217–227 in the N-terminal side of SMD3, and 304–316 in $SMD4_{JM}$ inhibit to various degrees AngII-induced GTPase activity of isolated vascular smooth muscle membrane [9]. This indicates that these segments constitute, at least in part, G protein interaction sites for AT_1R. Our data now show that the full SMD2 and SMD3, and a.a. 309–327 on $SMD4_{JM}$ can all interact with CaM at physiological Ca^{2+} concentrations. This suggests that CaM binding at these locations may interfere with G protein coupling. Consistently, Zhang et al. have shown *in vitro* that CaM can compete with peptides corresponding to a.a. 215–232 on SMD3 and a.a. 305–317 on $SMD4_{JM}$ for interaction with $G_{\beta\gamma}$ subunit [32]. It has been postulated that CaM interaction with SMDs in GPCRs could interfere with G protein coupling via two mechanisms prevention of G protein-receptor preassociation or promotion of dissociation [25]. Given multi-site interactions between CaM and AT_1R with disparate Ca^{2+} sensitivities, both mechanisms might be in play. For example, with the ability to interact with a.a. 215–242 (SMD3) at resting Ca^{2+} levels, CaM interaction here might prevent $G_{\beta\gamma}$ preassociation at rest. On the other hand, CaM binding at a.a. 125–241 (SMD2) and a.a. 309–327 on $SMD4_{JM}$ may promote $G_{\beta\gamma}$ dissociation upon AT_1R stimulation.

The downstream functional impact of CaM binding to AT_1R in living cells has not been studied. Inhibition of CaM using W-7 in primary vascular smooth muscle cells virtually abolishes AngII-induced ERK1/2 phosphorylation. Consistently, mutagenesis data indicate that reduction in CaM binding affinity and Ca^{2+} sensitivity for interaction at each identified domain is associated with significantly reduced AT_1R-mediated ERK1/2 phosphorylation. In addition, AngII-induced Ca^{2+} signals are also significantly reduced in cells expressing mKate2-AT_1R with mutant sequence at each domain. In our Ca^{2+} measurements, cells heterologously expressing a mutant AT_1R were recognized by mKate2 fluorescence and selected prior to switching to fura-2 channel, so that the measured signals reflect effect of the intended expressed receptor. Furthermore, the presence of some non-transfected cells in the same microscopic field (absence of mKate2 fluorescence) allowed for comparing Ca^{2+} signals from cells expressing or not expressing exogenous AT_1R in the same experiments. Interestingly, reduced CaM binding at a.a. 125–141 (SMD2) drastically alters the dynamics

of AngII-induced Ca^{2+} signal, from a typical transient into a slow-rising, low amplitude signal. This finding first confirms that signals from the expressed receptors dominated over any endogenous AT_1R in this system. However, the finding is surprising considering the lower affinity, dynamic range and Ca^{2+} sensitivity of CaM interaction with SMD2 than with the other two locations. We do not know the explanation for this. Speculatively, given proximity of the submembrane domains in cells, CaM binding at SMD2 might affect associations at the other domains and thus have impact in cells beyond what biochemical properties of its interaction with SMD2 in isolation would predict. While this is an attractive hypothesis, it is technically challenging at present to test in cells, given that insertion of reporters in an SMD is likely to alter the relative association of binding partners to the remaining SMDs substantially.

In conclusion, AT_1R possesses up to three CaM-binding domains located at a.a. 125–141 (SMD2), 215–242 (SMD3), and 309–327 ($SMD4_{JM}$). These domains interact with CaM with disparate affinities and Ca^{2+} sensitivities in the physiological range of Ca^{2+} signals in cells. CaM interaction with SMD3 can occur at resting Ca^{2+} concentration. Functionally, interaction at each domain is important for AngII-stimulated Ca^{2+} signaling and ERK1/2 phosphorylation.

Acknowledgments

This study was supported by National Institutes of Health Grant HL112184 and Iowa Osteopathic and Educational Research Funds to QK-T. We thank Vahe Matnishian and Briana Gebert-Oberle for assistance in some experimental paradigms.

References

1. Ali MS, Sayeski PP, Dirksen LB, Hayzer DJ, Marrero MB, Bernstein KE. Dependence on the motif YIPP for the physical association of Jak2 kinase with the intracellular carboxyl tail of the angiotensin II AT1 receptor. J Biol Chem. 1997; 272:23382–23388. [PubMed: 9287353]
2. Aricescu AR, Lu W, Jones EY. A time- and cost-efficient system for high-level protein production in mammalian cells. Acta crystallographica. Section D, Biological crystallography. 2006; 62:1243–1250. [PubMed: 17001101]
3. Becamel C, Alonso G, Galeotti N, Demey E, Jouin P, Ullmer C, Dumuis A, Bockaert J, Marin P. Synaptic multiprotein complexes associated with 5-HT(2C) receptors: a proteomic approach. EMBO J. 2002; 21:2332–2342. [PubMed: 12006486]
4. Black DJ, LaMartina D, Persechini A. The IQ domains in neuromodulin and PEP19 represent two major functional classes. Biochemistry. 2009; 48:11766–11772. [PubMed: 19877718]
5. Black DJ, Tran QK, Persechini A. Monitoring the total available calmodulin concentration in intact cells over the physiological range in free Ca2+ Cell Calcium. 2004; 35:415–425. [PubMed: 15003851]
6. Bockaert J, Fagni L, Dumuis A, Marin P. GPCR interacting proteins (GIP). Pharmacol Ther. 2004; 103:203–221. [PubMed: 15464590]
7. Bofill-Cardona E, Kudlacek O, Yang Q, Ahorn H, Freissmuth M, Nanoff C. Binding of calmodulin to the D2-dopamine receptor reduces receptor signaling by arresting the G protein activation switch. J Biol Chem. 2000; 275:32672–32680. [PubMed: 10926927]
8. Bolzon BJ, Cheung DW. Isolation and characterization of single vascular smooth muscle cells from spontaneously hypertensive rats. Hypertension. 1989; 14:137–144. [PubMed: 2474494]
9. Kai H, Alexander RW, Ushio-Fukai M, Lyons PR, Akers M, Griendling KK. G-Protein binding domains of the angiotensin II AT1A receptors mapped with synthetic peptides selected from the receptor sequence. Biochem J. 1998; 332(Pt 3):781–787. [PubMed: 9620883]

10. Kakiuchi S, Yasuda S, Yamazaki R, Teshima Y, Kanda K, Kakiuchi R, Sobue K. Quantitative determinations of calmodulin in the supernatant and particulate fractions of mammalian tissues. J Biochem (Tokyo). 1982; 92:1041–1048. [PubMed: 7174634]
11. Kendall RT, Strungs EG, Rachidi SM, Lee MH, El-Shewy HM, Luttrell DK, Janech MG, Luttrell LM. The beta-arrestin pathway-selective type 1A angiotensin receptor (AT1A) agonist [Sar1,Ile4,Ile8]angiotensin II regulates a robust G protein-independent signaling network. J Biol Chem. 2011; 286:19880–19891. [PubMed: 21502318]
12. Kim SA, Heinze KG, Waxham MN, Schwille P. Intracellular calmodulin availability accessed with two-photon cross-correlation. Proc Natl Acad Sci U S A. 2004; 101:105–110. [PubMed: 14695888]
13. Leik CE, Willey A, Graham MF, Walsh SW. Isolation and culture of arterial smooth muscle cells from human placenta. Hypertension. 2004; 43:837–840. [PubMed: 14967841]
14. Luby-Phelps K, Hori M, Phelps JM, Won D. Ca(2+)-regulated dynamic compartmentalization of calmodulin in living smooth muscle cells. J Biol Chem. 1995; 270:21532–21538. [PubMed: 7665565]
15. Mahon MJ, Shimada M. Calmodulin interacts with the cytoplasmic tails of the parathyroid hormone 1 receptor and a sub-set of class b G-protein coupled receptors. FEBS Lett. 2005; 579:803–807. [PubMed: 15670850]
16. Marsault R, Murgia M, Pozzan T, Rizzuto R. Domains of high Ca2+ beneath the plasma membrane of living A7r5 cells. Embo J. 1997; 16:1575–1581. [PubMed: 9130702]
17. Mehta PK, Griendling KK. Angiotensin II cell signaling: physiological and pathological effects in the cardiovascular system. Am J Physiol Cell Physiol. 2007; 292:C82–97. [PubMed: 16870827]
18. Minakami R, Jinnai N, Sugiyama H. Phosphorylation and calmodulin binding of the metabotropic glutamate receptor subtype 5 (mGluR5) are antagonistic in vitro. J Biol Chem. 1997; 272:20291–20298. [PubMed: 9242710]
19. Paradis P, Dali-Youcef N, Paradis FW, Thibault G, Nemer M. Overexpression of angiotensin II type I receptor in cardiomyocytes induces cardiac hypertrophy and remodeling. Proc Natl Acad Sci U S A. 2000; 97:931–936. [PubMed: 10639182]
20. Persechini A. Monitoring the intracellular free Ca(2+)-calmodulin concentration with genetically-encoded fluorescent indicator proteins. Methods Mol Biol. 2002; 173:365–382. [PubMed: 11859776]
21. Shen X, Valencia CA, Szostak JW, Dong B, Liu R. Scanning the human proteome for calmodulin-binding proteins. Proc Natl Acad Sci U S A. 2005; 102:5969–5974. [PubMed: 15840729]
22. Thomas WG, Pipolo L, Qian H. Identification of a Ca2+/calmodulin-binding domain within the carboxyl-terminus of the angiotensin II (AT1A) receptor. FEBS Lett. 1999; 455:367–371. [PubMed: 10437806]
23. Tran QK, Black DJ, Persechini A. Intracellular coupling via limiting calmodulin. J Biol Chem. 2003; 278:24247–24250. [PubMed: 12738782]
24. Tran QK, Black DJ, Persechini A. Dominant affectors in the calmodulin network shape the time courses of target responses in the cell. Cell Calcium. 2005; 37:541–553. [PubMed: 15862345]
25. Tran QK, Firkins R, Giles J, Francis S, Matnishian V, Tran P, VerMeer M, Jasurda J, Burgard MA, Gebert-Oberle B. Estrogen Enhances Linkage in the Vascular Endothelial Calmodulin Network via a Feedforward Mechanism at the G Protein-Coupled Estrogen Receptor 1. J Biol Chem. 2016; 291:10805–10823. [PubMed: 26987903]
26. Tran QK, VerMeer M, Burgard MA, Hassan AB, Giles J. Hetero-oligomeric Complex between the G Protein-coupled Estrogen Receptor 1 and the Plasma Membrane Ca2+-ATPase 4b. J Biol Chem. 2015; 290:13293–13307. [PubMed: 25847233]
27. Tran QK, VerMeer M. Biosensor-based approach identifies four distinct calmodulin-binding domains in the G Protein-Coupled Estrogen Receptor 1. PloS one. 2014; 9:e89669. [PubMed: 24586950]
28. Turner JH, Gelasco AK, Raymond JR. Calmodulin interacts with the third intracellular loop of the serotonin 5-hydroxytryptamine1A receptor at two distinct sites: putative role in receptor phosphorylation by protein kinase C. J Biol Chem. 2004; 279:17027–17037. [PubMed: 14752100]

29. Ulrich-Merzenich G, Metzner C, Bhonde RR, Malsch G, Schiermeyer B, Vetter H. Simultaneous isolation of endothelial and smooth muscle cells from human umbilical artery or vein and their growth response to low-density lipoproteins. In Vitro Cell Dev Biol Anim. 2002; 38:265–272. [PubMed: 12418923]

30. Wang D, Sadee W, Quillan JM. Calmodulin binding to G protein-coupling domain of opioid receptors. J Biol Chem. 1999; 274:22081–22088. [PubMed: 10419536]

31. Wu X, Bers DM. Free and bound intracellular calmodulin measurements in cardiac myocytes. Cell Calcium. 2007; 41:353–364. [PubMed: 16999996]

32. Zhang R, Liu Z, Qu Y, Xu Y, Yang Q. Two Distinct Calmodulin Binding Sites in the Third Intracellular Loop and Carboxyl Tail of Angiotensin II (AT1A) Receptor. PloS one. 2013; 8:e65266. [PubMed: 23755207]

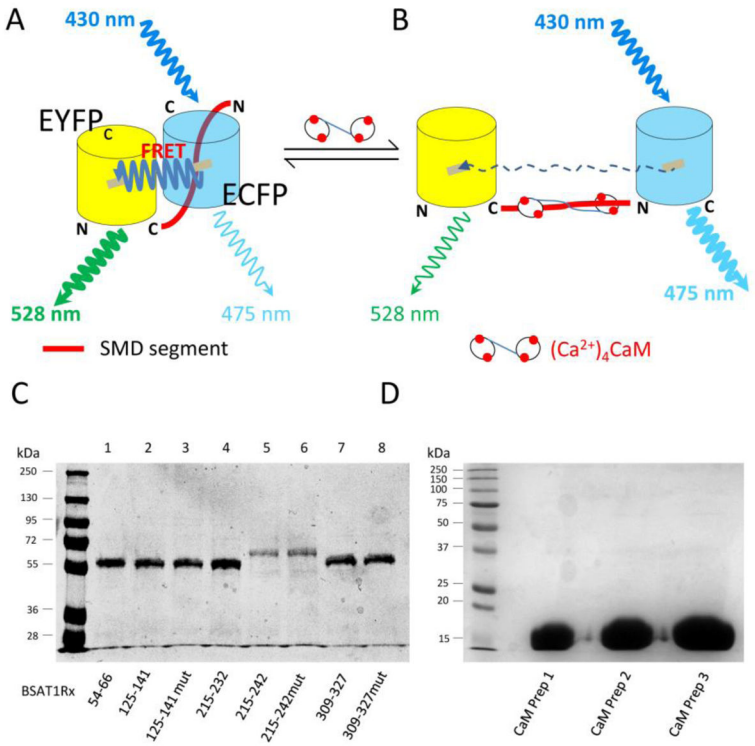

Fig. 1.

Method to screen for CaM binding domains in AT_1R. (A & B) Design of FRET biosensors to screen for CaM interaction (see text for explanation), depicted in unbound (A) and CaM-bound (B) conditions. $EYFP_C$, citrine enhanced yellow fluorescence protein; ECFP, enhanced cyan fluorescence protein; N and C, N-terminal and C-terminal ends, respectively, of fluorophores. (C) Representative Coomassie gel of the biosensors generated. (D) Coomassie gel of three separate CaM preps.

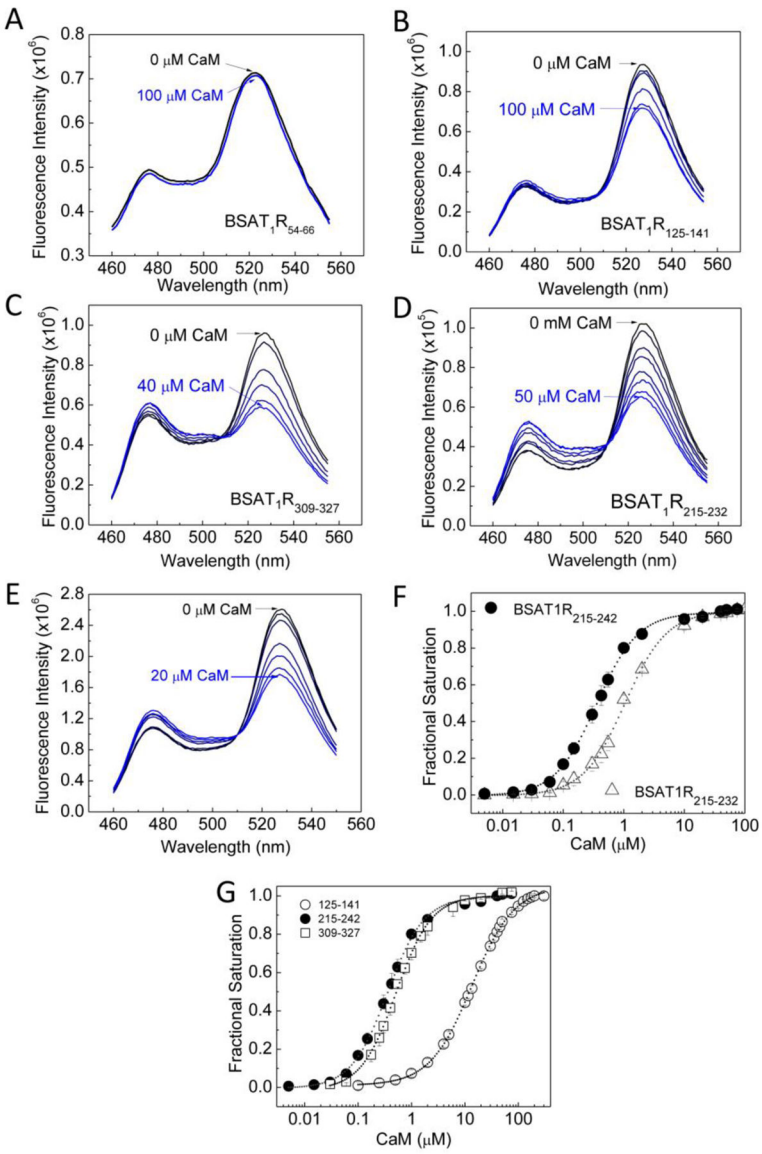

Fig. 2.

CaM-binding domains in AT_1R. Incremental purified CaM was titrated as the emission spectra of $BSAT_1R_{54–66}$ (A), $BSAT_1R_{125–141}$ (B), $BSAT_1R_{309–327}$ (C), $BSAT_1R_{215–232}$ (D), and $BSAT_1R_{215–242}$ (E) were monitored. Initial reaction mix contained 0.5 μM $BSAT_1R_X$, 0.1mg/ml BSA and 1 mM Ca^{2+} in titration buffer (F) Composite plot showing difference in binding affinity for CaM between $BSAT_1R_{215–232}$ (open triangles) and $BSAT_1R_X$ (closed circles). (G) Composite plot of average (n = 6 independent experiments) fractional saturations of $BSAT_1R_{125–141}$, $BSAT_1R_{215–242}$, and $BSAT_1R_{309–327}$ as a function of Ca^{2+}-liganded CaM.

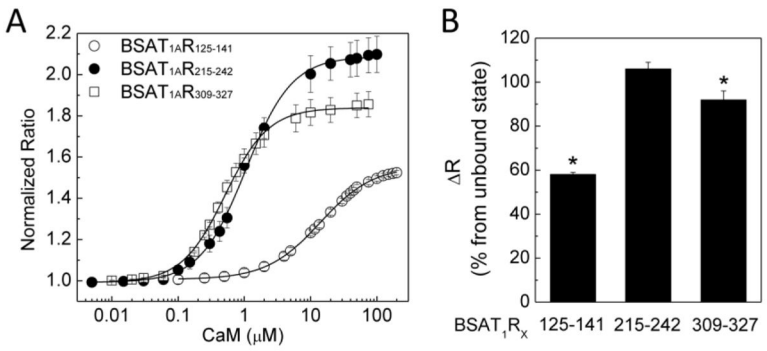

Fig. 3.

Dynamic ranges of $BSAT_1R_X$. (A) Relative average ratios of $BSAT_1R_{125–141}$, $BSAT_1R_{215–242}$, and $BSAT_1R_{309–327}$ in response to Ca^{2+}-liganded CaM titration. (B) Average per cent increase from unbound state in ratio of $BSAT_1R_X$. n = 6 independent experiments. *, $p<0.05$ vs value for $BSAT_1R_{215–242}$

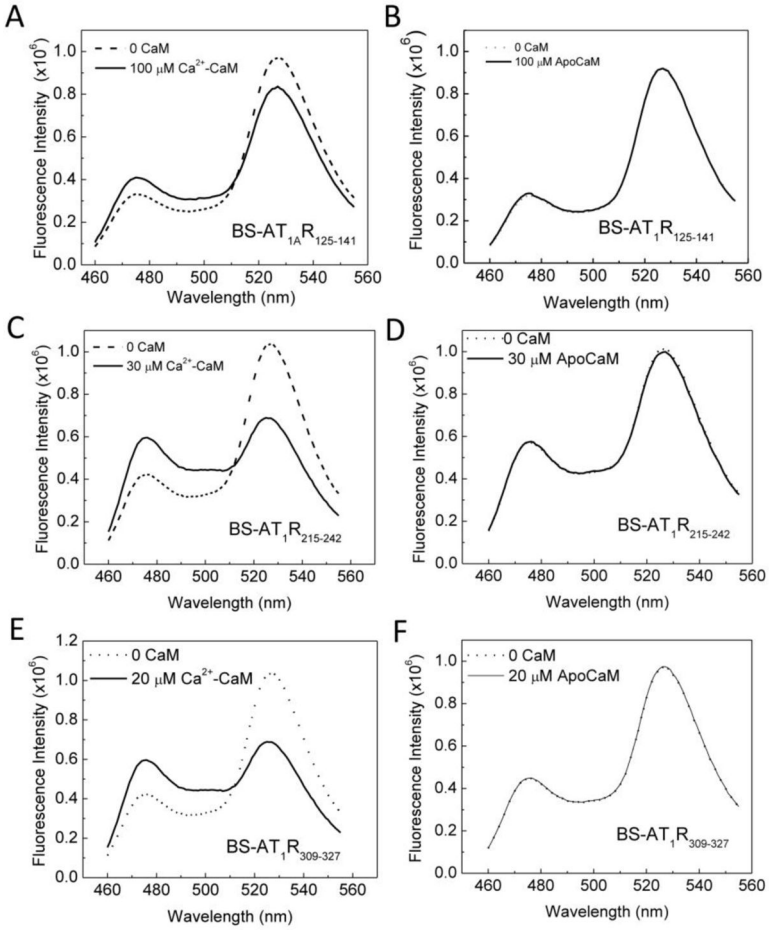

Fig. 4.

Ca^{2+} dependency of interactions between $BSAT_1R_X$ and CaM. Specified concentrations of CaM (saturating concentrations determined from K_d titrations) were added to a mixture of 0.5 μM $BSAT_1R_{125–141}$, $BSAT_1R_{215–242}$, $BSAT_1R_{309–327}$ in titration buffer containing 0.1 mg/ml BSA and 1 mM Ca^{2+} (A, C, E, respectively) or absence of Ca^{2+} (apoCaM) and presence of 0.25 mM BAPTA (B, D, F, respectively). Dotted and solid spectra, $BSAT_1R_X$ response before and after the addition of CaM, respectively. Data are representative of 6 independent experiments for each paradigm.

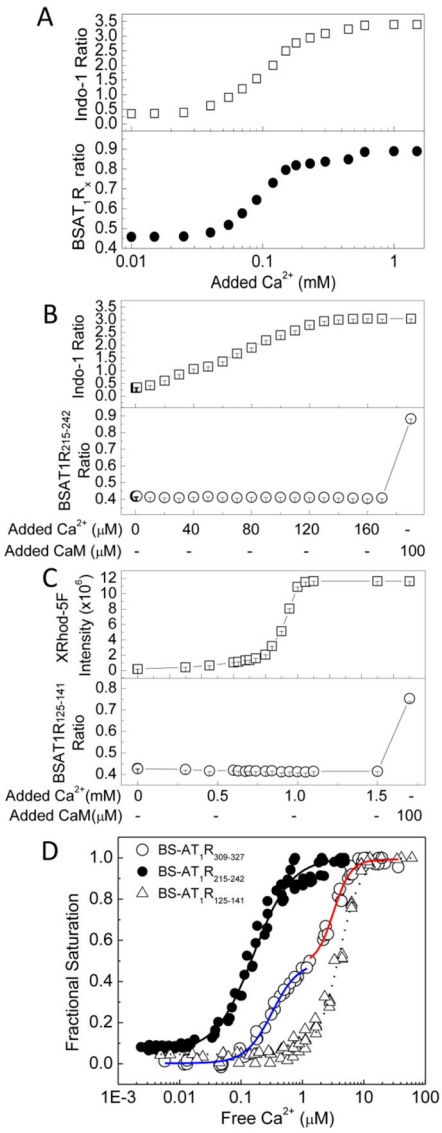

Fig. 5.

Determinations of the Ca^{2+} sensitivities of AT_1R-CaM interactions. (A) Typical experiment to determine EC50(Ca^{2+}) value for $BSAT_1R_X$-CaM interaction. Reactions contained 0.5 μM $BSAT_1R_X$, 2 μM Indo-1 (or XRhod-5F), 0.25 mM BAPTA, and saturating CaM concentration (obtained from K_d titrations). Incremental aliquots of Ca^{2+} were added as the emission intensities of Indo-1 (upper panel) and $BSAT_1R_X$ responses (lower panel) were monitored. (B and C) Controls for bleed-through artifact between indo-1 or XRhod-5F and $BSAT_1R_x$. Reactions contained 0.1 μM $BSAT_1R_{215–242}$ and 2 μM indo-1 (B) or 0.1 μM $BSAT_1R_{125–141}$ and 2 μM XRhod-5F (C) in the presence of 0.25 mM BAPTA. Incremental aliquots of Ca^{2+} were added as indo-1, XRhod-5F and biosensor fluorescence responses were monitored. 100 μM purified CaM was added after indo1 and XRhod-5F signals had been saturated. (D) Aggregate (n = 3) plots showing Ca^{2+} sensitivity of the interactions between CaM $BSAT_1R_{125–141}$ (open triangles), $BSAT_1R_{215–242}$ (closed circles), and $BSAT_1R_{309–327}$ (open circles). Fractional $BSAT_1R_X$ response and free Ca^{2+} were calculated

as described under Materials and Methods. Fits were performed on aggregate data from three independent experiments. Blue and red fits, CaM-BSAT$_1$R$_{309–327}$Sp1 and CaM-BSAT$_1$R$_{309–327}$Sp2, respectively (see text for explanation). Data were from 3 independent experiments for each biosensor.

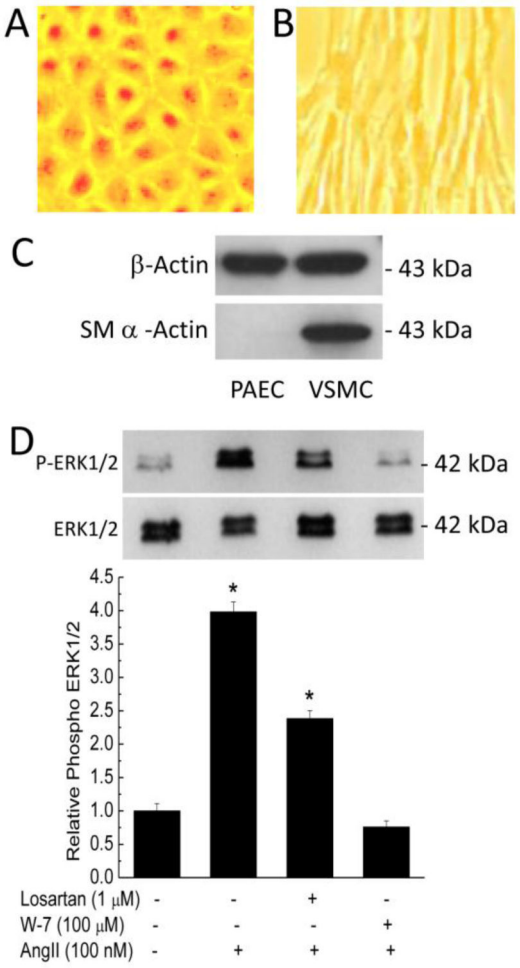

Fig. 6.

AngII-induced ERK1/2 phosphorylation in primary VSMCs and effects of CaM antagonism. (A & B) Bright-field images of primary porcine endothelial cells (PAECs, A) and VSMCs (B) isolated from the same porcine aortas cultured in phenol red-containing medium for visualization purposes. Images were taken using a Moticam CMOS camera (Motic Microscopes). (C) Immunoblots for smooth muscle α-actin (lower) and β-actin (upper) from lysates of the PAECs and VSMCs isolated. (D) Primary VSMCs were serum starved for 4 hrs prior to pretreatment with or without losartan (1 μM) or W-7 (100 μM) for 30 minutes, followed by treatment for 10 minutes with vehicle or 100 nM AngII. Upper immunoblot, representative changes in phosphorylated ERK1/2; lower immunoblot, corresponding total ERK1/2 expression, reprobed from stripped upper membrane. Histogram, average (n = 6 independent experiments) relative AT_1R-mediated ERK1/2 phosphorylation in response to specified treatment. Densitometric values of the phosphorylated ERK1/2 bands were divided by corresponding values for total ERK1/2 bands and normalized.

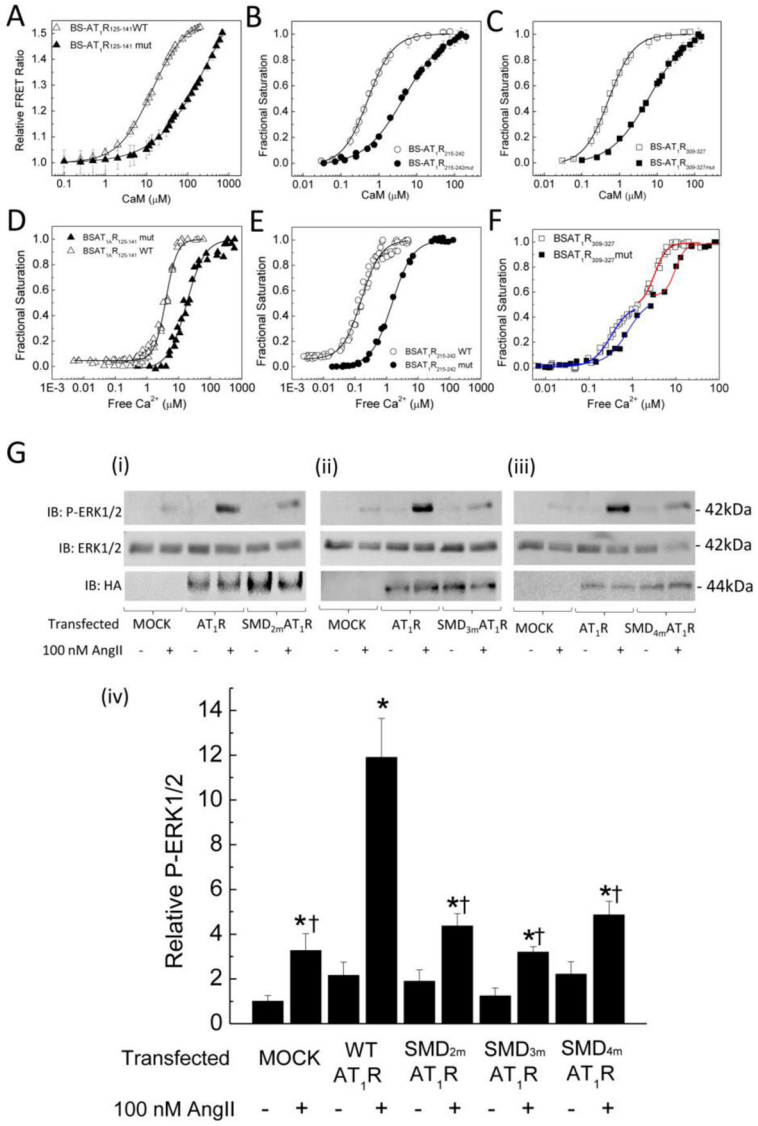

Fig. 7.

Effects of CaM binding-reducing mutations on AT_1R-mediated signaling. (A, B, C) Average (n = 6 independent experiments) responses of the specified $BSAT_1R_X$ with wild-type (open symbols) or mutant (closed symbols) sequences at the identified CaM binding domain as a function of free CaM showing reduction in binding affinities. Conditions for titration reactions were as described for Fig. 2. Plot data were fit to Eq. 2 or 3 to yield K_d values (Table-4). (D, E, F) Average (n = 6 independent experiments) fractional saturations of the specified $BSAT_1R_X$ with wild-type (open symbols) or mutant (closed symbols) sequences in the identified CaM-binding domains in the presence of saturating CaM and incremental free Ca^{2+} measured as described in Fig. 5. Data were fit to Eq. 6 to yield EC50(Ca^{2+}) values (Table-4). Blue and red fits correspond to wild-type or mutant CaM-$BSAT_1R_{309–327}$Sp1 and CaM-$BSAT_1R_{309–327}$Sp2, respectively. (G) HEK293 cells were transfected as indicated with mock materials or plasmids encoding hemagglutinin (HA) epitope tagged to the N termini of full-length AT_1R with wild-type or mutant sequences (Table-2) in SMD2 (i), SMD3 (ii), or

$SMD4_{JM}$ (iii). 24 hrs post-transfection, cells were serum starved for 4 hrs, followed by treatment with vehicle or 100 nM AngII for 10 minutes. Upper and middle immunoblots, representative phosphorylated ERK1/2 and total ERK1/2 from the same SDS-PAGE membranes; lower immunoblots, expression of HA-AT_1R across corresponding samples. (iv) Average (n = 6 independent experiments) relative phosphorylated ERK1/2. Relative densitometric values of phosphorylated ERK1/2 bands were divided by corresponding values for the total ERK1/2 bands and normalized to corresponding mock-untreated values. *, $p<0.05$ vs corresponding untreated conditions; †, $p<0.05$ vs valuesfrom cells transfected with full-length wild-type AT_1R and treated with AngII.

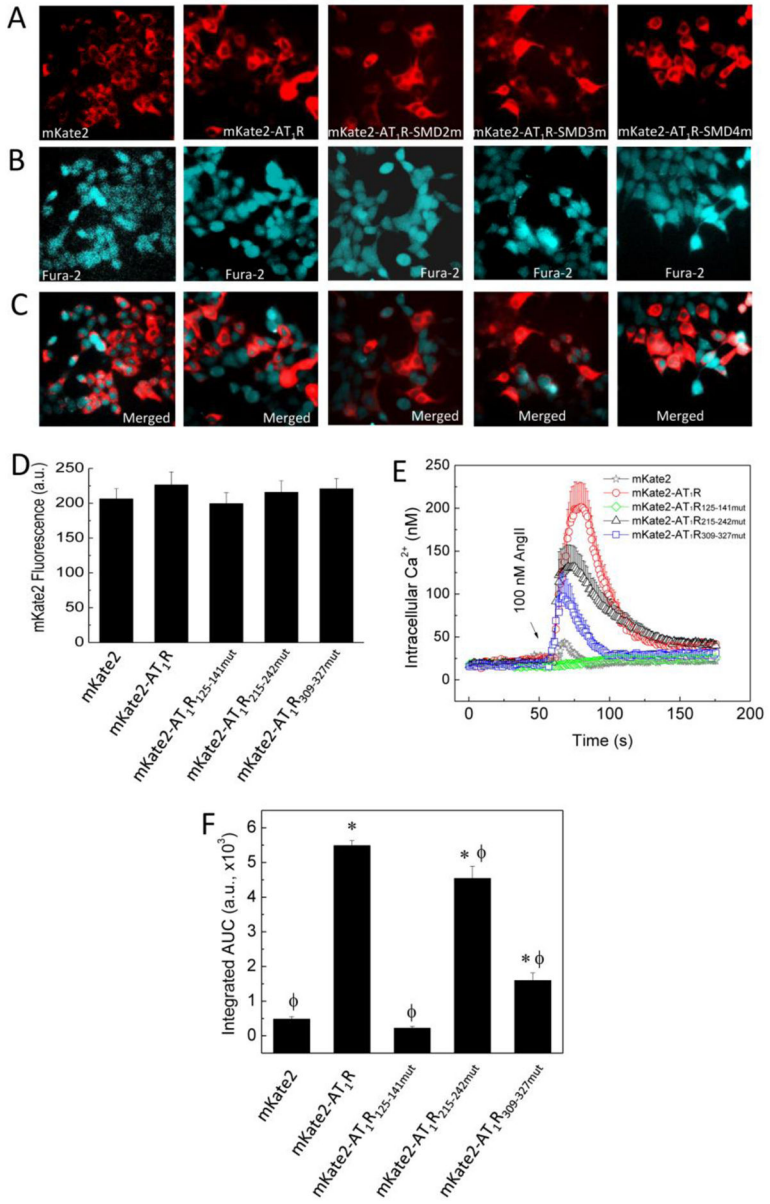

Fig. 8.

Effects of reduced CaM binding at individual SMDs on AngII-induced Ca^{2+} signals. HEK293 cells expressing plasmids encoding mKate2 alone or in fusion with the N terminus of full-length AT_1R with wild-type or mutant sequence at SMD2, or $SMD4_{JM}$ were loaded with fura-2/AM as described under Materials and Methods. (A) Epifluorescence of mkate2 moiety. (B) Corresponding epifluorescence of fura-2 in the same microscopic field. (C) Merged mKate2 and fura-2 fluorescence images. (D) Average mKate2 fluorescence intensities of all individual cells selected for Ca^{2+} measurements. (E) Average time courses of Ca^{2+} signals stimulated by AngII as indicated. (F) Corresponding average total integrated areas under curve (AUC). N = 60 cells from 6 independent experiments for each paradigm; *

and ϕ, $p < 0.05$ vs AUC values of cells expressing mKate2 only and mKate2-wildtype AT_1R fusion, respectively.

Table 1

Primers

Fragment generated	Forward primer	Reverse primer
BamHI-AT_1R-Stop-XhoI	CTCGGGATCCATGATTCTCAACTCTTC	CTCGCTCAAGTCACTCAACCTCAAAAC
KpnI-mKate2-BamHI	CGACGGTACCATGTCAGAACTTATCAAGGA	CGC TGG ATC CTC TGT GCC CCA GTT T
KpnI-$AT_1R_{52–64}$-AgeI	CTCGGGTACCGTCATTTACTTTTATAT	CTCGACCGGTACTGGCCACAGTCTTCA
KpnI-$AT_1R_{125–141}$-AgeI	CTCGGGTACCGATCGATACCTGGCTAT	CTCGACCGGTTGTGCGTCGAAGGCG
KpnI-$AT_1R_{215–232}$-AgeI	CTCGGGTACCTATACTCTTATTTGG	CTCGACCGGTTTTGTTCTTCTTCTGAATTTC
KpnI-$AT_1R_{215–242}$-AgeI	CTCGGGTACCTATACTCTTATTTGG	CTCGACCGGTAATTATCTTAAAAAT
KpnI-$AT_1R_{309–327}$-AgeI	CTCGGGTACCTTTAAAAGATATTTT	CTCGACCGGTGTGGGATTTGGCTTTTGG
KpnI-$AT_1R_{304–323}$-AgeI	CTC GGG TAC CTT TCT GGG GAA AAA A	CTC GAC CGG TTT TTG GGG GAA TAT A
KpnI-$AT_1R_{305–327}$-AgeI	CTC GAC CGG TCT GGG GAA AAA ATT T	CTC GAC CGG TGT GGG ATT TGG CTT TTG G
KpnI-$AT_1R_{328–359}$-AgeI	CTCGGGTACCTCAAACCTTTCAACAAAA	CTCGACCGGTGAATTCCTCAACCTCAAAACATGGTGC
KpnI-$AT_1R_{125–141mut}$-AgeI	CTGTGGTACCGATCAAGCCCTGGC	CTGGACCGGTTGTTTGTCGAAGTTGGG
KpnI-$AT_1R_{215–242mut}$-AgeI	CAGCGGTACCTATACTCTTATTGCG	CGCCACCGGTAATTATCTTAGCAAT
KpnI-$AT_1R_{309–327mut}$-AgeI	CGCTGGTACCGCTAAAAGATATGCTC	GCTACCGGTGTGGGATTGGGCTTTT

Table 2

Substitutions in AT_1R's CaM-binding domains

Domain targeted	Wild-type sequence	Mutant sequence
SMD2 ($AT_1R_{125–141}$)	DRYLAIVHPMKSRLRRT	D***QA***LAIVHPMKS***Q***LR***Q***T
SMD3 ($AT_1R_{215–242}$)	YTLIWKALKKAYEIQKNKPRNDDIFKII	YTLI***A***KALKKA***A***EIQKN***Q***PRNDDI***A***KII
$SMD4_{JM}$ ($AT_1R_{309–327}$)	FKRYFLQLLKYIPPKAKSH	***A***KRY***A***LQLLK***A***IPPKA***Q***SH

Table 3

Gblock gene fragments. Substitutions from wild-type sequenced are in bold-face fonts and italicized. Identified CaM binding domain sequences are underlined.

AT_1R Fragment	gBlock sequence	Restriction enzymes to clone to full-length AT_1R
125–141 mut	CTACTCACGTGTCTCAGCATTGAT***CAAGCC***CTGGCTATTGTTCACCCAATG AAGTCC***CAA***CTTCGA***CAA***ACAATGCTTGTAGCCAAAGTCACCTGCATCAT CATTTGGCTGCTGGCAGGCTTGGCCAGTTTGCCAGCTATAATCCATCGAA ATGTATTTTTCATTGAGAACACCAATATTACAGTTTGTGCTTTCCATTATG AGTCCCAAAATTCAACCCTCCCGATAGGGCTGGGCCTGACCAAAAATATA CTGGGTTTCCTGTTTCCTTTTCTGATCATTCTTACAAGTTATACTCTTATTG CGAAGGCCCTAAAGAAGGCTTATGAAAT	PmlI – EcoNI
215–242 mut	CAGCATTGATCGATACCTGGCTATTGTTCACCCAATGAAGTCCCGCCTTC GACGCACAATGCTTGTAGCCAAAGTCACCTGCATCATCATTTGGCTGCTG GCAGGCTTGGCCAGTTTGCCAGCTATAATCCATCGAAATGTATTTTTCATT GAGAACACCAATATTACAGTTTGTGCTTTCCATTATGAGTCCCAAAATTC AACCCTCCCGATAGGGCTGGGCCTGACCAAAAATATACTGGGTTTCCTGT TTCCTTTTCTGATCATTCTTACAAGTTATACTCTTATT***GCG***AAGGCCCTAA AGAAGGCT***GCT***GAAATTCAGAAGAAC***CAA***CCAAGAAATGATGATATT***GC*** ***T***AAGATAATTATGGCAATTGTGCTTTTCTTTTTCTTTTCCTGGATTCCCCAC CAAATATTCACTTTTCTGGATGTATTGATTCAACTAGGCATCATACGTGAC TGTAGAATTGCAGATATTGTGGACACGGCCATGCCTATCACCATTTGTAT AGCTTATTTTAACAATTGCCTGAATCCTCTTTTTTATGGCTTTCTGGGGAA AAAATTTAAAAGATATTTTCTCCAGCTTCTAAAATATATTCCCCCAAAAG CCAAATCCCACTCAAACCTTTCAACAAAAATGAGCACGCTTTCCTACCGC CCCTCAGATAATGTAAGCTCATCCACCAAGAAGCCTGCACCATGTTTTGA GGTTGAGTGACTCGAGCATGCATC	ClaI – XhoI
309–327 mut	GAAGGCCCTAAAGAAGGCTTATGAAATTCAGAAGAACAAACCAAGAAAT GATGATATTTTTAAGATAATTATGGCAATTGTGCTTTTCTTTTTCTTTTCCT GGATTCCCCACCAAATATTCACTTTTCTGGATGTATTGATTCAACTAGGCA TCATACGTGACTGTAGAATTGCAGATATTGTGGACACGGCCATGCCTATC ACCATTTGTATAGCTTATTTTAACAATTGCCTGAATCCTCTTTTTTATGGC TTTCTGGGGAAAAAA***GCT***AAAAGATAT***GCT***CTCCAGCTTCTAAAA***GCT***AT TCCCCCAAAAGCC***CAA***TCCCACTCAAACCTTTCAACAAAAATGAGCACGC TTTCCTACCGCCCCTCAGATAATGTAAGCTCATCCACCAAGAAGCCTGCA CCATGTTTTGAGGTTGAGTGACTCGAGCATGCATC	EcoNI – XhoI

Table 4

Apparent K_d, EC50(Ca^{2+}) and DR values for CaM interactions with $BSAT_1R_X$

$BSAT_1R_X$	Apparent K_d (μM)	EC50(Ca^{2+}) (μM)		Dynamic Range
$BSAT_1R_{125–141}$	13.9 ± 0.39 *	4.10 ± 0.11 *		1.58 ± 0.01 *
$BSAT_1R_{125–141mut}$	> 318 ± 13.0 †	17.6 ± 0.78 †		1.34 ± 0.01 *
$BSAT_1R_{215–232}$	1.05 ± 0.04 *	0.30 ± 0.03 *		2.41 ± 0.03
$BSAT_1R_{215–242}$	0.36 ± 0.05	0.15 ± 0.01		2.06 ± 0.03
$BSAT_1R_{215–242mut}$	4.52 ± 0.25 †	1.49 ± 0.03 †		1.55 ± 0.01 †
$BSAT_1R_{309–327}$	0.51 ± 0.01	Sp1	Sp2	1.92 ± 0.04
		0.31 ± 0.02 *	3.17 ± 0.2 *	
$BSAT_1R_{309–327mut}$	6.60 ± 0.18 †	Sp1mut	Sp2mut	1.47 ± 0.01 †
		0.77 ± 0.1 †	9.6 ± 0.49 †	

* $p < 0.05$ vs corresponding value of $BSAT_1R_{215–242}$;

† $p < 0.05$ vs corresponding value of wild-type $BSAT_1R_X$;